RESEARCH PAPER

Direct Shear Creep Characteristics of Sand Treated with Microbial-Induced Calcite Precipitation

Jie Yuan[1] · Donglin Lei[1] · Yi Shan[1] · Huawei Tong[1] · Xiaotian Fang[2] · Jitong Zhao[1]

Abstract
Microbial-induced calcite precipitation (MICP) is a promising method to improve geotechnical engineering properties. In this context, little research has been conducted on the creep behavior of MICP-treated sand. Therefore, the present work performed direct shear creep tests to investigate the creep-related mechanical properties of silica sand and calcareous sand grouted three, six, and nine times in the MICP treatment. Compared to the untreated sand, the creep deformation of the MICP-treated silica sand grouted three and six times was more significant, and the creep deformation of the MICP-treated silica sand grouted nine times decreased by 88.0%, indicating that the treatment of the silica sand with the MICP could reduce its creep deformation. The creep deformation of the MICP-treated calcareous sand was larger than that of the untreated calcareous sand except for the sample grouted three times which had a creep deformation equivalent to that of the untreated calcareous sand, implying that the treatment of the calcareous sand with the MICP could increase its creep deformation. The scanning electron microscopy (SEM) images demonstrated that the calcium carbonate produced by microorganisms in the voids formed a connection between the sand particles as the critical factor affecting the creep behavior of the MICP-treated silica sand. In the case of the calcareous sand, the cavities were filled up with calcium carbonate, which decreased the effect of the interlocking structure of the sand particles.

Keywords Microbial-induced calcite precipitation (MICP) · Direct shear creep · Silica sand · Calcareous sand · Creep deformation

1 Introduction

Microbial-induced calcite precipitation (MICP) and enzymatically induced calcite precipitation (EICP) are new soil reinforcement technology improving the physical and mechanical properties of sand [1]. MICP and EICP treatments have the characteristics of little energy consumption, negligible disturbance to a foundation, and minimal environmental pollution [2]. Whiffin [3], an Australian geological engineer, first proposed microbial-induced calcite precipitation. The chemical reactions of the hydrolysis of urea are expressed in Eqs. (1) and (2) [4]:

$$CO(NH_2)_2 + H_2O \rightarrow CO_3^{2-} + 2NH_4^+ \qquad (1)$$

$$Ca^{2+} + CO_3^{2-} \rightarrow CaCO_3 \qquad (2)$$

Many recent studies have reported that the treatment of sand with MICP and EICP can effectively enhance its mechanical properties, such as strength and stiffness [5–8], can decrease its permeability [9–12], can increase its

✉ Yi Shan
yshan@gzhu.edu.cn

Jie Yuan
yuanj@gzhu.edu.cn

Donglin Lei
2111916123@e.gzhu.edu.cn

Huawei Tong
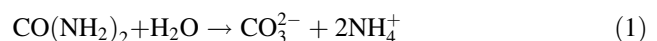tonghw@gzhu.edu.cn

Xiaotian Fang
fangxt@szgas.com.cn

Jitong Zhao
2111816008@e.gzhu.edu.cn

[1] Department of Civil Engineering, Guangzhou University, Guangzhou 510006, China

[2] Shenzhen Gas Corporation Ltd., Shenzhen 518049, China

resistance to liquefaction [13–15], and can enhance its anti-scour/anti-erosion performance [16]. MICP and EICP can also be applied to expansive soils [17], fine-grained soils [4], and silty sand [18]. All the above studies indicate that, as a new technology for the reinforcement of foundations, MICP can efficaciously reinforce the mechanical properties of sand foundations.

As a type of time-dependent deformation behavior, creep is defined as the strain increasing with time at constant stress. The time-dependent behavior of soil is also an essential phenomenon from the engineering point of view. In this context, the creep behavior of soil leads to severe geotechnical problems, such as residual settlement [19], landslides [20], and failure [21], which pose a threat to people's production and life. Although the creep behavior of sand is less remarkable than that of clay, many tests and accidents have proved that sand also has creep characteristics. For example, Briaud and Gibbens [22] and Burland et al. [23] found that the foundation built on a gravel layer had a large creep settlement. Du et al. [24] developed a creep model of sand particles and a mechanism for the landslide caused by fatigue liquefaction. Therefore, it is necessary to study the creep characteristics of sand.

Some recent studies have demonstrated that the treatment of sand with microbial-induced calcite precipitation can affect its deformation behavior under stress. Arboleda-Monsalve et al. [25] reported a significant reduction in soil compressibility after the MICP treatment. They stated that the measured axial strain of the biologically treated samples was minimal for the vertical effective stress stages below 200 kPa compared to that of the untreated control specimens. Xiao et al. [26] also found that the specimens with a higher $CaCO_3$ content were less compressible than those with lower $CaCO_3$ content. The untreated specimen presented the most considerable vertical strain (23.42%) at a stress of 30 MPa compared to the specimen containing 2.49% $CaCO_3$ with a smaller vertical strain of 22.72%. In another work, Feng and Montoya [27] reported that the cementation samples treated with microbial-induced calcite precipitation tended to show a dilative volumetric strain even when the confinement increased to 400 kPa. In contrast, the untreated sample exhibited a contractive behavior during shearing.

The present research aimed to understand the creep characteristics of MICP-treated sand. Thus, we explored the creep characteristics and changes in the microscopic void structure of MICP-treated sand. For this purpose, a series of direct shear creep tests was carried out to investigate the creep-related mechanical properties of the sand treated with microbial-induced calcite precipitation. The interfacial mechanism of the MICP-treated sand was examined using scanning electron microscopy (SEM), and the characteristics of the microscopic voids of the MICP-

treated sand were analyzed. This study attempted to provide a theoretical basis for the long-term settlement deformation of field MICP-treated sand.

2 Materials and Methods

2.1 Materials
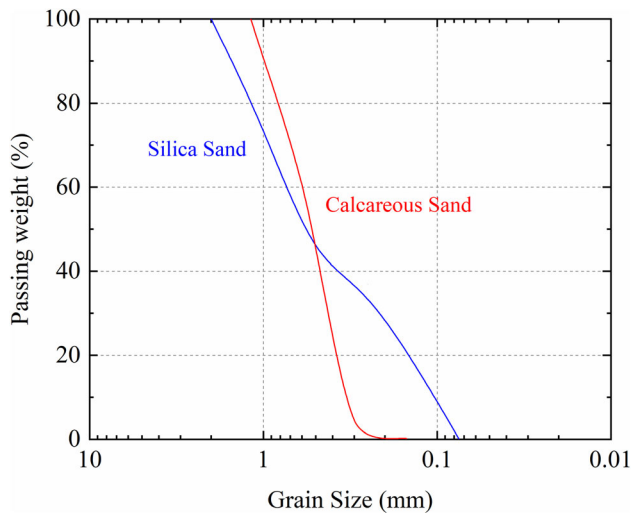
2.1.1 Silica Sand and Calcareous Sand

Silica sand compliant with ISO standards and calcareous sand from Yongxing Islands located in the South China Sea were chosen for the experiments. Table 1 lists the physical and mechanical parameters of the silica sand and the calcareous sand, and Fig. 1 delineates their grain size distribution curves. The scanning electron microscopy observation demonstrates that the surface of the silica sand (Fig. 2a) is smooth and flat, with only a few small potholes and no internal void structure. The calcareous sand has a rough and porous surface with irregular pores having a large edge angle. Moreover, the calcareous sand particles are distributed with honeycomb structures, as shown in Fig. 2b.

2.2 Bacterial Culture and Cementation Solution

The *Bacillus pasteurii* (DSM33 Netherlands) was used in this study. *Bacillus pasteurii* is a urea hydrolysis bacterium that can hydrolyze urea to form carbonate ions and thus induce calcite precipitation. It was necessary to culture the *Bacillus pasteurii* strain before treating the sand with the microbial-induced calcite precipitation. To this end, a sterilized culture medium comprising 20 g/L yeast extract, 10 g/L $(NH_4)_2SO_4$, and 2 g/L NaOH was used, and the pH of the medium was set at about 9. The culture medium was first sterilized at a temperature of 120 °C for 20 min to prevent contamination with unwanted foreign species. The bacteria were cultured in a conical flask under a shaking speed of 160 rpm, a temperature of 30 °C, and a period of 24 h. The bacterial cell concentration was quantified by measuring the absorbance (optical density) of the suspension using a spectrophotometer [8]. The optical density of the bacterial solution measured at a wavelength of 600 nm (OD_{600}) ranged from 0.8 to 1.0. The conductivity-measuring medium measured the specific urease activity of the bacteria to hydrolyze urea. To this end, 2 mL of the bacterial suspension was added to 18 mL of 1.1 M urea (urea reaction concentration of 1 M), and the change in the relative conductivity (mS/min) was recorded over 5 min at 26 °C. In the measured range of activities, 1 mS/min correlated with a hydrolysis activity of 11 (mM urea)/min [28]. The specific urease activity calculated by dividing the

Table 1 The physical and mechanical parameters of the silica sand and the calcareous sand

Property	G_s	d_{10} (mm)	d_{30} (mm)	d_{60} (mm)	C_u	C_c	e_{max}	e_{min}
Silica sand	2.653	0.126	0.162	0.562	4.47	0.37	0.950	0.605
Calcareous sand	2.76	0.269	0.316	0.366	1.36	1.02	1.24	0.8

Fig. 1 Grain size distributions curves of the silica sand and the calcareous sand

urease activity by OD_{600} was approximately 4.5 mM urea/min/OD. Table 2 also presents the ingredients of the cementation solution.

2.3 Specimens Preparation

2.3.1 Specimen Parameters

Cylindrical specimens with a diameter of 61.8 mm and a height of 20 mm were used for the direct shear creep tests. The D_r of the specimens was controlled at 50% using 89.49 g of the silica sand and 81.93 g of the calcareous sand to exclude the influence of the water content and the void ratio. The dry deposition method was adopted to prepare the specimens, which simulated a relatively homogeneous soil condition. The specimens were divided into three layers into the mold, and each layer was slightly compacted with a compaction tool [7]. Furthermore, the sand used in the test was sterilized at a temperature of 108 °C for 60 min to avoid the influence of other bacteria on the test results.

2.3.2 Grouting Procedure

At present, MICP grouting reinforcement methods chiefly include the soaking method [29], the mixing method [30, 31], and the intermittent cyclic grouting method [32, 33]. This work adopted the intermittent cyclic grouting
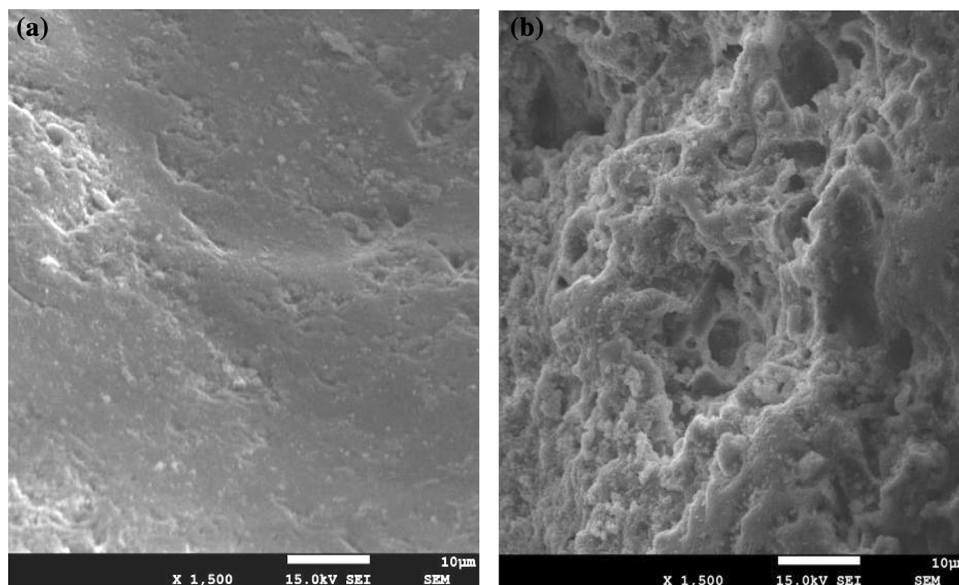

Fig. 2 Scanning electron microscopy images of **a** silica sand and **b** calcareous sand
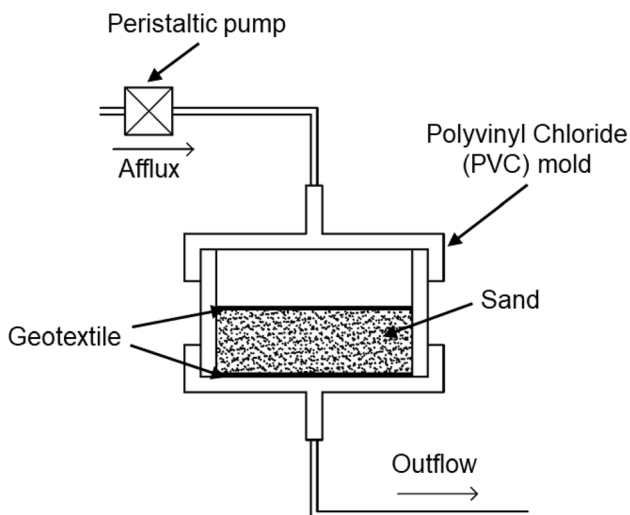
Table 2 The ingredients of the cementation solution

Reagent	Urea	CaCl₂	NaHCO₃	NH₄Cl	Nutrient broth
Concentration (g/L)	30	55	2.12	10	3

method [32]. Figure 3 depicts a schematic diagram of the grouting procedure, and Fig. 4 illustrates the grouting reinforcement procedure consisting of one injection of the bacterial solution and five injections of the cementation solution. Moreover, the grouting rate was set at 3 mL/min, and the specimens were prepared at room temperature, approximately 25 °C.

2.4 Experimental Method

2.4.1 Direct Shear Creep Test

An improved triplex rheology direct shear test apparatus [34] based on the Model ZLB-1 triplex rheology direct shear test apparatus (Nanjing Soil Instrument Factory Co., Ltd., China) conforming to the Chinese standard for geotechnical test method [35] was employed to analyze the direct shear creep of the specimens, as shown in Fig. 5. It could maintain the humidity of the specimens by regularly adding water. In addition, the direct shear creep test adopted the graded loading method, and the shear strength of the sand and MICP-treated sand determined the loading increment of the direct shear creep test, as tabulated in Table 3 [36]. The samples included untreated sand and MICP-treated sand. Table 4 presents the scheme of the direct shear creep test. For the untreated sample and the sample grouted three times, the fifth stage loading was set as 200 kPa, respectively, by rounding up to the nearest hundredth of the minimum shear strength. The sixth stage
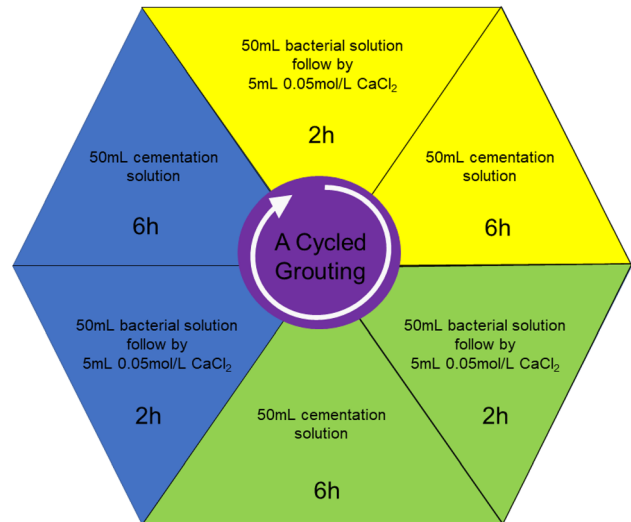
Fig. 4 Procedure for the grouting reinforcement

Fig. 5 Improved triplex rheology direct shear creep apparatus: 1: indicators of shearing force; 2: moisturizing seal box; 3: indicators of normal and shear displacements; 4: normal load; 5: shear box; 6: shear load

loading of the sample grouted three times was also set as 240 kPa. For the samples grouted six and nine times, the maximum loading was set as 500 kPa by rounding up to the nearest hundredth of the minimum shear strength. The shear loading in each stage also increased equally according to the maximum loading stage and the number of stages. A dynamometer determined the actual shear loading of each stage. The experimental data were reported in chronological order 0 min, 1 min, 2 min, 15 min, 1 h, 2 h,

Fig. 3 Schematic diagram of the grouting procedure

Table 3 The shear strength of the untreated sand and the sand treated with the microbial-induced calcite precipitation

Group	Test ID	Vertical pressure and shear strength (kPa)				Cohesion and friction angle	
		100	200	300	400	c (kPa)	φ (°)
Silica sand	S-DSC0	72.2	135.4	205.3	272.30	3.90	33.8
	S-DSC3	111	206.3	301.6	396.80	15.73	43.6
	S-DSC6	297.233	484.083	670.933	857.78	110.38	61.9
	S-DSC9	458.403	630.321	802.239	974.16	286.49	59.8
Calcareous sand	C-DSC0	57.35	111	156.325	207.20	9.25	26.3
	C-DSC3	108.17	202.47	296.77	391.07	13.87	43.3
	C-DSC6	237.8	323	408.2	493.40	152.60	40.4
	C-DSC9	566.64	667.28	767.92	868.56	466.00	45.2

Table 4 The scheme of the direct shear creep test

Group	Test ID	Number of grouting	Consolidation pressure (kPa)	Horizontal shear stress (kPa)					
				1	2	3	4	5	6
Silica sand	S-DSC$_0$-4	0	400	39	79	115	162	199	–
	S-DSC$_3$-4	3		38	81	124	163	192	247
	S-DSC$_6$-4	6		51	150	250	350	450	500
	S-DSC$_9$-4	9		52	152	249	350	450	500
Calcareous sand	C-DSC$_0$-4	0	400	38	79	123	163	199	–
	C-DSC$_3$-4	3		39	79	121	163	201	249
	C-DSC$_6$-4	6		52	150	250	350	450	500
	C-DSC$_9$-4	9		50	150	249	350	452	501

3 h, 6 h, 12 h, and 24 h. Furthermore, the standard for the creep stability is that the shear displacement is no more than 0.005 mm/day under each shear load, and after reaching the standard creep deformation stability, the next loading stage can be entered.

2.4.2 Scanning Electron Microscopy

After the direct shear creep tests, the SEM (JEOL JSM-7001F, Japan) images of the representative MICP-treated sand specimens were captured. The samples were dried at a temperature of 100 °C and coated with gold using a sputter coating to improve the quality and resolution of the SEM images.

3 Results

3.1 Direct Shear Creep Test Results

3.1.1 Creep Characteristics of Untreated Sand

Figure 6a illustrates the variation in the shear strain of the silica sand with time at various shear stress stages, that is, the shear strain–time curves. With an increase in the shear stress, the creep behavior of the silica sand increase, and the samples show different creep laws. At low shear stress, i.e., the first two stages of the shear stress, the immediate deformation and creep deformation of the sample are small, and the deformation of the sample does not increase remarkably with time, indicating a stable creep composed of only the immediate deformation and the constant-rate deformation. From the third stage of the shear stress, the creep deformation rises with an increase in the shear stress, and the decay time of the creep rate is short. It can also be seen in Fig. 6a that the silica sand begins to show a considerable creep behavior when the shear stress is equal to 162 kPa.

Figure 6b delineates the shear strain–time relationship of the calcareous sand. The creep deformation of the calcareous sand increases with the enlargement of the shear stress. Moreover, at various shear stresses, the immediate deformation and creep deformation of the specimen are small, implying the characteristics of a stable creep.

Subtracting the minimum strain from the maximum strain in the isochronous stress–strain curves of the untreated sand in Fig. 7 yields the variation in the shear creep strain with the shear stress stage, as plotted in Fig. 8. This figure reveals that the creep of the calcareous sand is less affected by the change of the shear stress stage than the
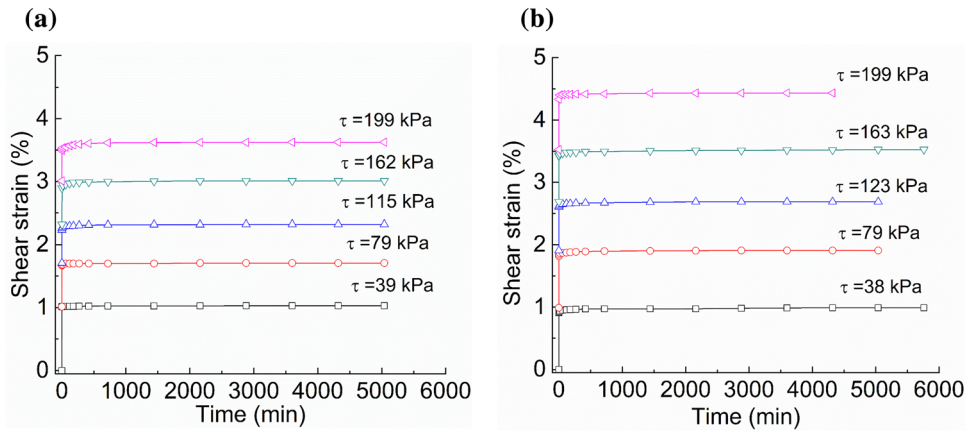
Fig. 6 Shear strain–time relationship of the untreated sand: **a** S-DSC$_0$-4; **b** C-DSC$_0$-4

silica sand. The creep deformation of the calcareous sand is larger than that of the silica sand under the action of low shear stress, i.e., the first and second stages of the shear stress. However, the trend is reversed under the action of high shear stress, that is, in stages three to five.

3.1.2 Creep Characteristics of MICP-Treated Sand

Figure 9 plots the variation in the shear strain with the time of the MICP-treated silica sand. Overall, the MICP-treated silica sand samples grouted three times do not have an apparent creep behavior, and the creep deformation enlarges with an increase in the shear stress. At low shear stress, i.e., the first and second stages of the shear stress, the samples show an immediate deformation after loading, and the creep deformation is small; indeed, the creep characteristics are not noticeable. The most considerable creep deformation occurs in the fifth shear stress stage, but it is smaller at the sixth stage of the shear stress. The MICP-treated silica sand samples grouted six times only show an immediate deformation after loading and do not experience a dramatic creep deformation in the first to fourth stages of
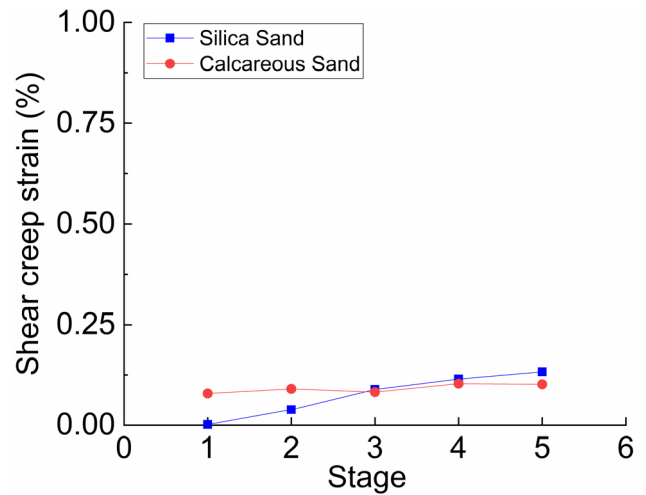

Fig. 8 Variation in the shear creep strain with the shear stress stage of the untreated sand

loading. A metastable creep appears from the fifth stage of loading. The MICP-treated silica sand samples grouted nine times do not experience a creep deformation until the
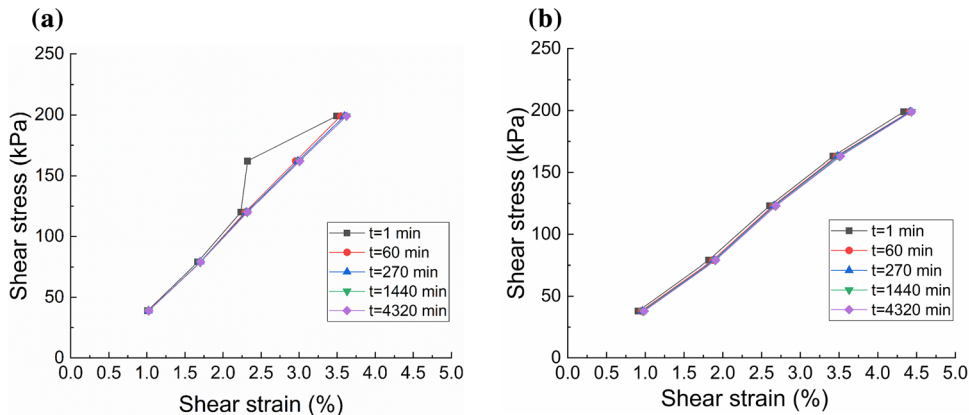

Fig. 7 Isochronous stress–strain curves of the untreated sand: **a** S-DSC$_0$-4; **b** C-DSC$_0$-4
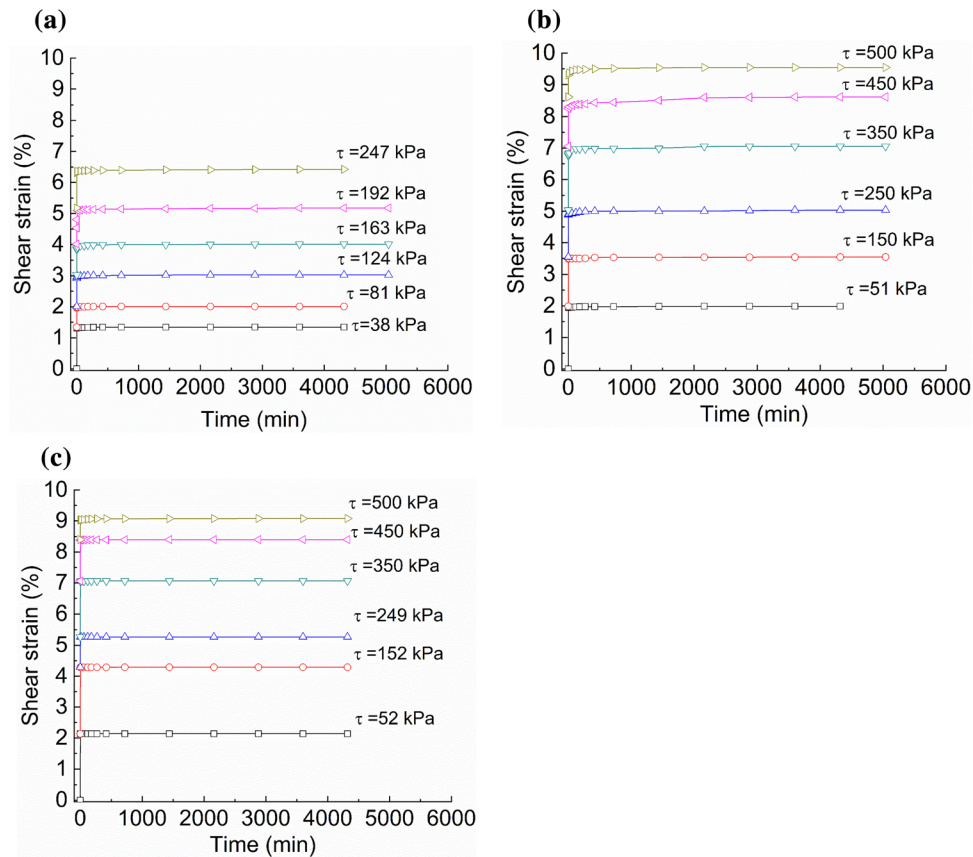
Fig. 9 Shear strain–time relationship of the MICP-treated silica sand: **a** S-DSC$_3$-4; **b** S-DSC$_6$-4; **c** S-DSC$_9$-4

sixth stage of the shear stress (500 kPa) and then have a slight deformation with the growth of the time after the immediate deformation. Therefore, the creep behavior of the MICP-treated silica sand samples grouted nine times is not remarkable, and they can show a specific attenuation creep characteristic only at high shear stress.

Figure 10 draws the isochronous stress–strain curves of the MICP-treated silica sand. The variation in the shear creep strain with the shear stress stage of the MICP-treated silica sand is also obtained from its isochronous stress–strain curves and compared with that of the silica sand in Fig. 11. Ignoring the data points of the fifth shear stress stage of the MICP-treated silica sand grouted three times in Fig. 11, the creep deformation of the specimen first enlarges and then decreases as the number of grouting rises to nine. The creep deformation of the samples grouted three and six times is more significant than that of the samples grouted nine times. At the fifth stage of the shear stress, the creep deformation of the samples grouted nine times is 0.016%, while that of the untreated silica sand is 0.133%, indicating a decrease of 0.117%. This reduction accounts for 88.0% of the creep deformation of the untreated silica sand.

Figure 12 delineates the shear strain–time relationship of the MICP-treated calcareous sand. The creep characteristics of the MICP-treated calcareous sand are similar to those of the MICP-treated silica sand. On the whole, compared with the MICP-treated silica sand with the same number of grouting, the instantaneous deformation of the MICP-treated calcareous sand is generally the same, but its creep deformation is more considerable.

Figure 13 depicts the isochronous stress–strain curves of the MICP-treated calcareous sand. Moreover, the shear creep strain variation with the shear stress stage of the MICP-treated calcareous sand obtained from the isochronous stress–strain curves is plotted and compared with that of the calcareous sand in Fig. 14. The creep deformation of the specimens grouted six and nine times is larger than that of the untreated calcareous sand. The creep deformation of the sample grouted three times is equivalent to that of the calcareous sand. In the fourth shear stress stage, the maximum creep deformation of the specimen grouted six times reaches around 0.65%, which is 6.5 times higher than that of the calcareous sand (about 0.10%).
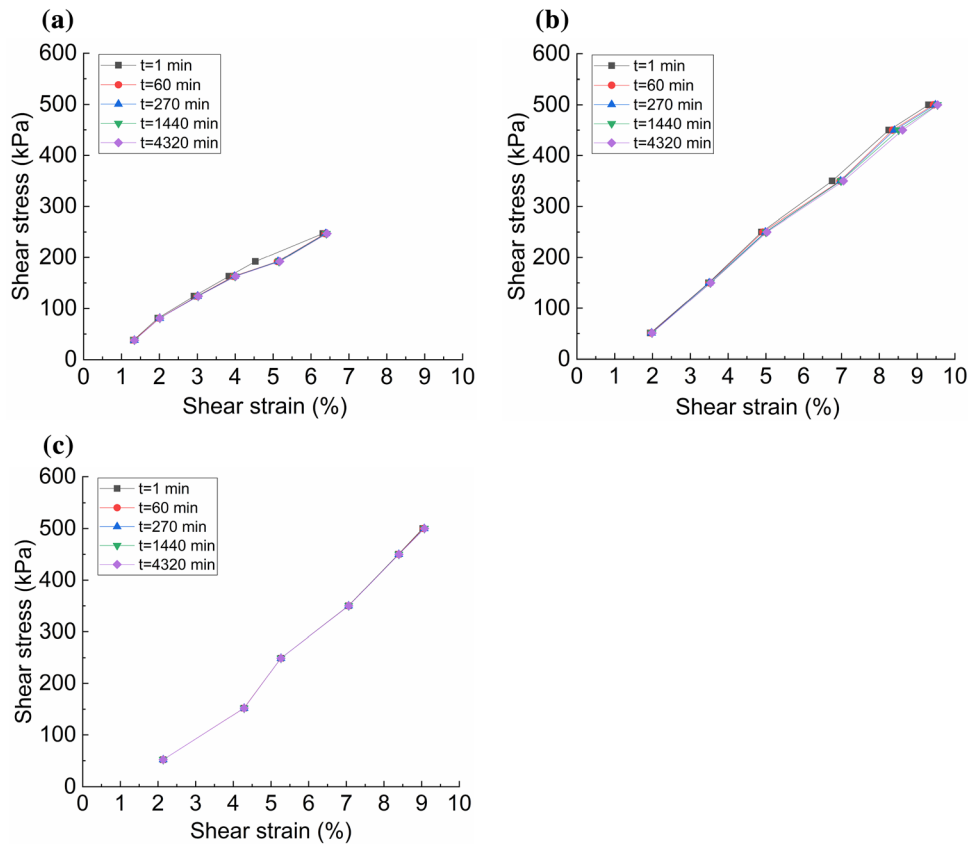
Fig. 10 Isochronous stress–strain curves of the MICP-treated silica sand: **a** S-DSC$_3$-4; **b** S-DSC$_6$-4; **c** S-DSC$_9$-4
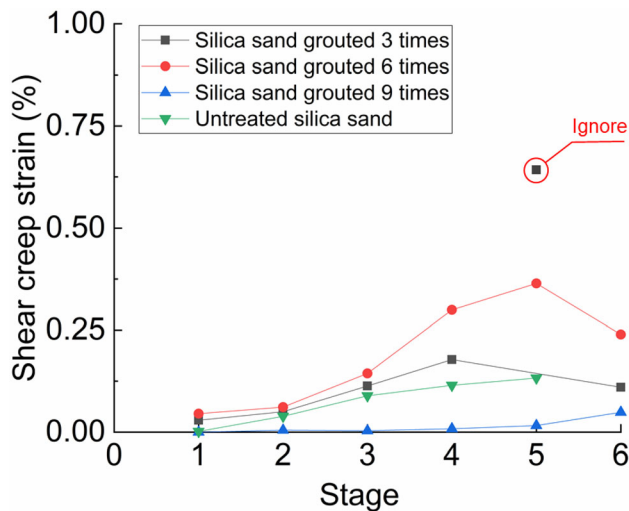

Fig. 11 Variation in the shear creep strain with the shear stress stage of the MICP-treated silica sand

3.2 Scanning Electron Microscopy Analysis

3.2.1 MICP-Treated Silica Sand

Figure 15 illustrates the SEM images of the MICP-treated silica sand. Figure 15a, b demonstrates that a small number of individual vaterite CaCO$_3$ crystals are formed on the smooth surface of the MICP-treated silica sand grouted three times; the CaCO$_3$ crystals have a small size. Figure 15c, d displays the SEM images of the MICP-treated silica sand specimens grouted six times. The section of the CaCO$_3$ crystal is destroyed in the creep shear process, and the connection comprises the calcite crystals accumulated by a large amount of CaCO$_3$. Furthermore, there are more and larger vaterite CaCO$_3$ crystals on the silica sand surface. Figure 15e, f depicts the SEM images of the specimens grouted nine times. The voids between the silica sand crystals can be observed, and there is a filling with a large amount of vaterite CaCO$_3$ accumulation in the voids.

3.2.2 MICP-Treated Calcareous Sand

Figure 16 shows the SEM images of the MICP-treated calcareous sand. According to Fig. 16a, b, there are many small cavities on the surface of the calcareous sand. CaCO$_3$ is formed in the holes of the calcareous sand particles grouted three times, but the holes are not filled up. Figure 16c, d displays the SEM images of the MICP-treated calcareous sand grouted six times. The calcareous sand surface is covered with CaCO$_3$ crystals, and the CaCO$_3$ is accumulated in the voids of the calcareous sand particles to
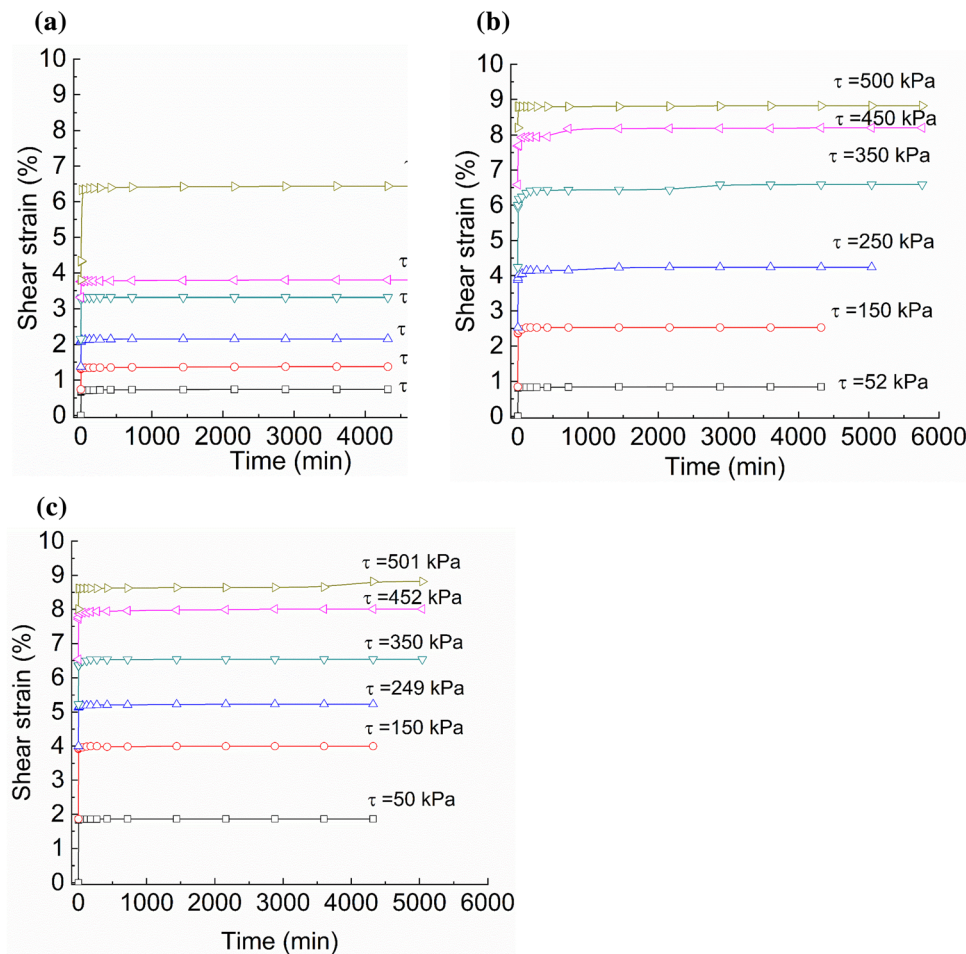
Fig. 12 Shear strain–time relationship of the MICP-treated calcareous sand: **a** C-DSC$_3$-4; **b** C-DSC$_6$-4; **c** C-DSC$_9$-4

form a connection. Figure 16e, f also depict the SEM images of the samples grouted nine times. It can be seen that the surface of the calcareous sand particles becomes smooth, and the larger surface cavities are filled up with the CaCO$_3$ crystals.

4 Discussion

The experimental results demonstrate that the creep behavior of the silica sand is different from that of the MICP-treated silica sand in a typical stress state. Compared with the silica sand, the creep deformation of the samples treated with microbial-induced calcite precipitation first enlarges and decreases as the MICP grouting increases. In addition, the creep behavior of the silica sand weakens after treating it with the microbial-induced calcite precipitation. Karimpour and Lade [37] believed that the creep characteristics of silica sand under normal stress are due to the combination of frictional sliding, the rearrangement of particles, and particle crushing. The frictional sliding

dominates the deformation under low stress, while the particle breakage produces the primary deformation under high stress.

Many researchers have confirmed that the calcite biofilms are generated after MICP treatment to wrap sand particles [38], and the pores in the soil are filled with calcium carbonate produced by the microbes [1]. The treatment of the sand with the microbial-induced calcite precipitation can effectively improve its shear-bearing capacity and affects its creep characteristics, because the calcium carbonate produced by microorganisms in the voids forms a connection between the sand particles, which bonds the particles together [39] and enhances the integrity of the sand. Comparing Fig. 2a with Fig. 15f reveals that the calcite biofilms are rougher than the surface of the silica sand particles. The covering layer of the calcite biofilm improves the surface roughness of the silica sand particles. Under the condition of low grouting, the calcium carbonate particles are small and dispersed (see Fig. 15a, b), and the voids between the sand particles are not filled up, which improves the bond between the sand particles.
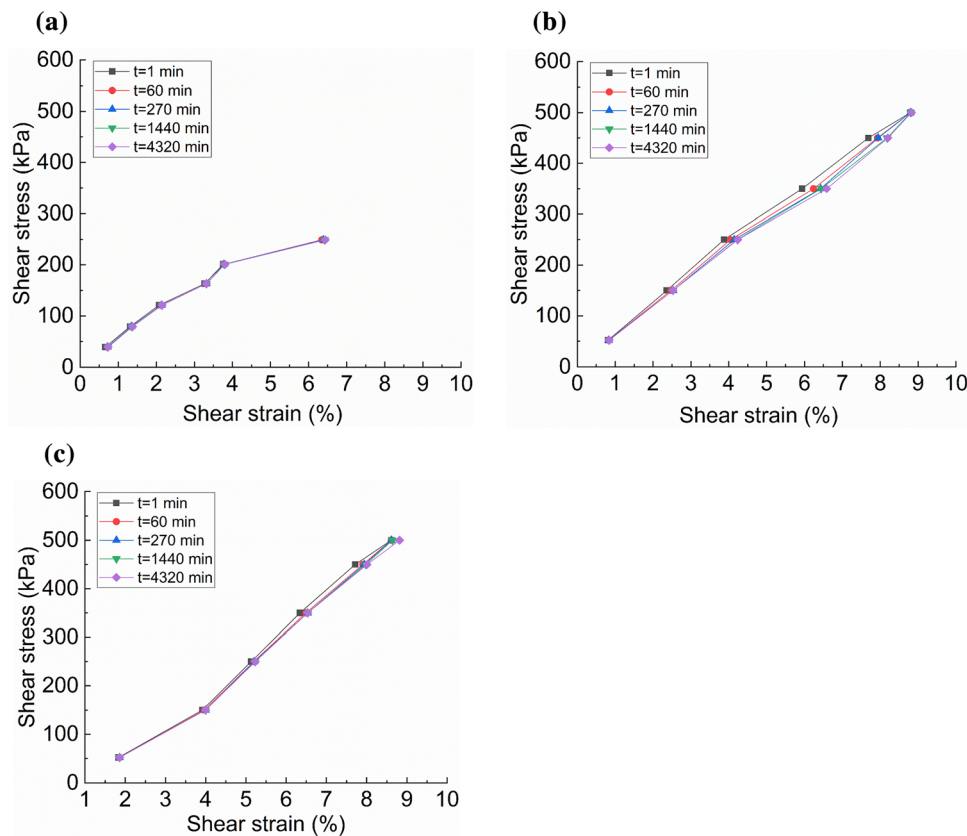
(a)

(b)

(c)

Fig. 13 Isochronous stress–strain curves of the MICP-treated calcareous sand: **a** C-DSC$_3$-4; **b** C-DSC$_6$-4; **c** C-DSC$_9$-4
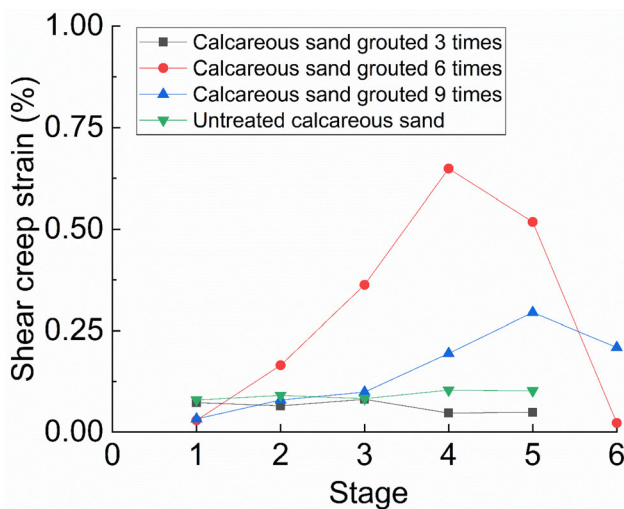

Fig. 14 Variation in the shear creep strain with the shear stress stage of the MICP-treated calcareous sand

However, under stress, the calcium carbonate connection between the silica sand particles breaks, resulting in a creep deformation and the rearrangement of the sand particles. Subsequently, because of the stress redistribution, these fragments may collapse again, leading to further creep deformation. As the number of grouting rises to, for example, six times, the production of calcium carbonate increases. The calcium carbonate accumulates in the voids between the silica sand particles to form a robust crystalloid connection. The smaller voids between the sand particles are filled up, while the larger ones still exist. Under the action of stress, the crystalloid connections are broken to form the calcium carbonate crystalloid particles (see Fig. 15c, d).

The silica sand particles have frictional sliding and can be rearranged, so the whole sample tends to a new stable state. At this time, the calcium carbonate crystalloid particles do not easily collapse again because of the stress redistribution, and the creep deformation of the sand does not simply develop further. The observed creep behavior may also be related to the mechanism illustrated in Fig. 17. However, at a higher number of grouting, the formation of the calcium carbonate further increases, so it accumulates at the joints between the sand particles to form robust crystalloid connections (see Fig. 15e, f). Moreover, the friction resistance and the cohesive force between the sand particles further improve, and the majority of the intergranular voids are filled up; thus, the porosity of the sand declines. After shear stress is applied to the sand, the sand particles experience a contact deformation, but they do not readily undergo a sliding deformation. Macroscopically,
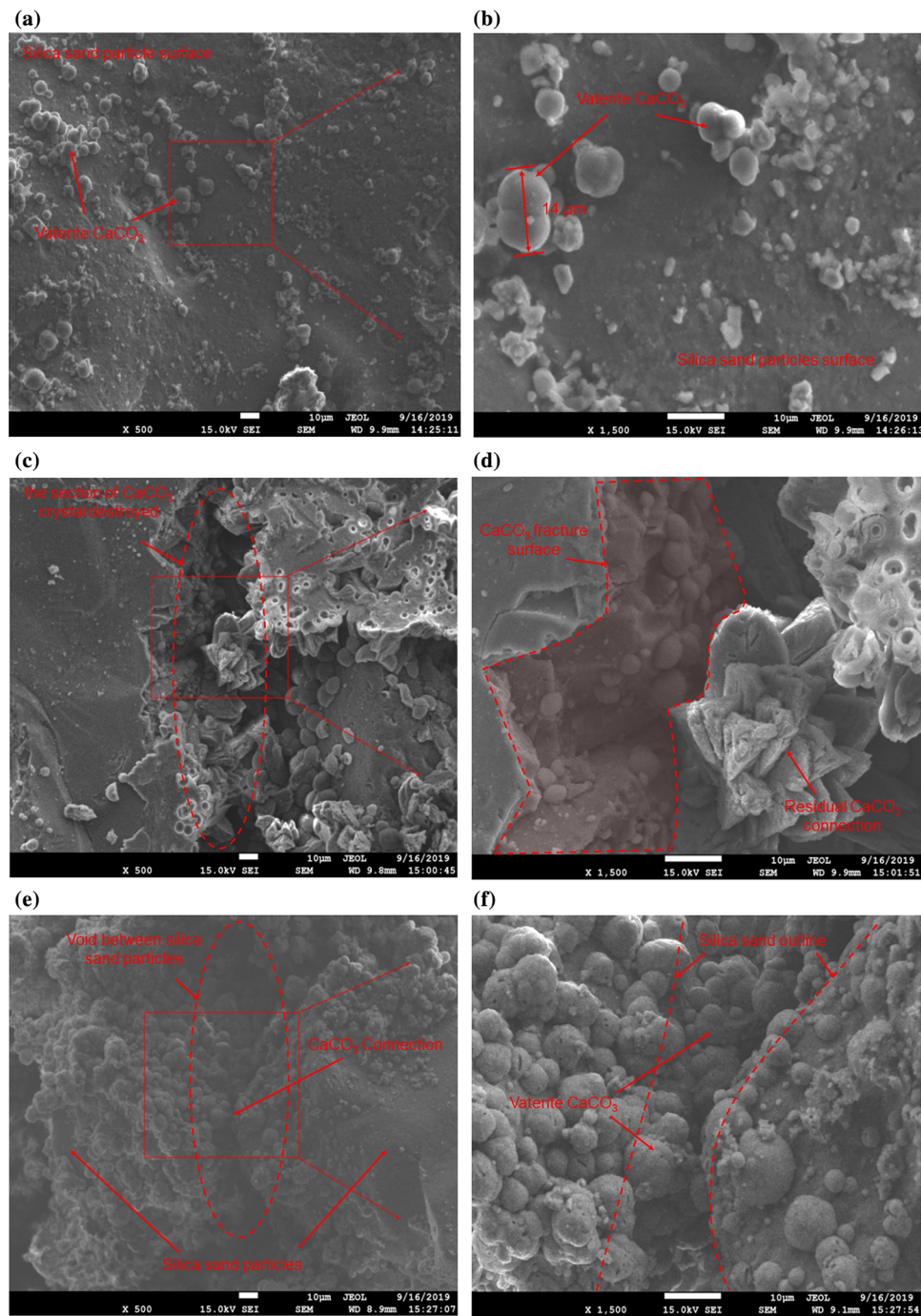
Fig. 15 SEM images of the MICP-treated silica sand: S-DSC$_3$-4 at a magnification of **a** × 500 and **b** × 1500; S-DSC$_6$-4 at a magnification of **c** × 500 and **d** × 1500; S-DSC$_9$-4 at a magnification of **e** × 500 and **f** × 1500

after an instantaneous deformation, the creep deformation of the sand tends to stabilize rapidly, and its creep behavior is not considerable.

The results demonstrate that the MICP-treated calcareous sand exhibits creep characteristics similar to the MICP-treated silica sand, but the creep of the MICP-treated calcareous sand is more remarkable than that of the silica sand. The rearrangement of the sand particles and the intergranular sliding under normal stress dominate the creep deformation of the calcareous sand. However, because of the rough surface of the calcareous sand particles, there are a large number of cavities, and the angular regions of some particles interlock with the cavities to form a relatively stable interlocking structure. The creep behavior of the calcareous sand is not noticeable, because the stable interlocking structure must collapse to produce
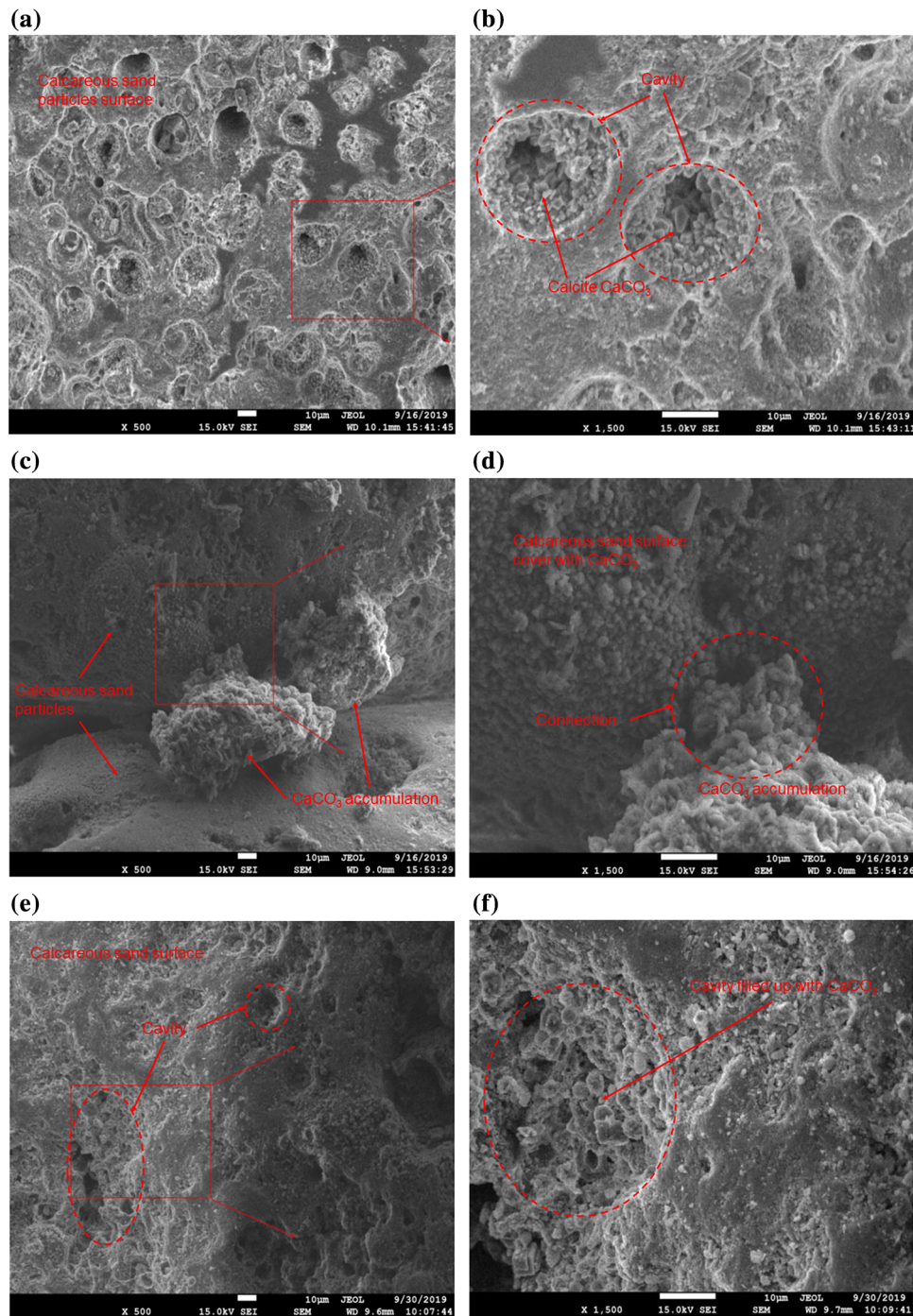
Fig. 16 SEM images of the MICP-treated calcareous sand: C-DSC$_3$-4 at a magnification of **a** × 500 and **b** × 1500; C-DSC$_6$-4 at a magnification of **c** × 500 and **d** × 1500; C-DSC$_9$-4 at a magnification of **e** × 500 and **f** × 1500

further plastic straining [40, 41]. Comparing Fig. 2b with Fig. 16a demonstrates that the cavities on the surface of the calcareous sand particles are filled up with the formed calcium carbonate after the treatment of the calcareous sand with the microbial-induced calcite precipitation. The interparticle friction of calcareous sand consists of the surface roughness and interlocking structure of its particles.

Therefore, the interlocking structure of the calcareous sand particles weakens, lessening the effects of the interparticle friction. After the shear stress destroys the calcium carbonate crystalloid connection, it is much easier for the sand particles to experience sliding deformation and the samples to show creep deformation. Therefore, the creep behavior of the MICP-treated calcareous sand is noticeable. The
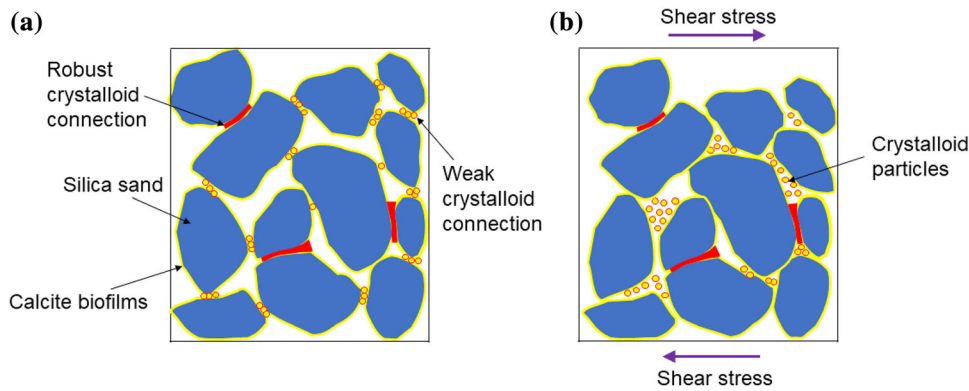
Fig. 17 Mechanisms of MICP-treated silica sand creep deformation **a** before loaded up to a given shear stress; **b** reach a new stable state

observed creep behavior may also be related to the mechanism illustrated in Fig. 18.

5 Conclusions

This work examined the creep-related mechanical properties of the sands treated with the microbial-induced calcite precipitation using a series of direct shear creep tests. The interfacial mechanism of the MICP-treated sands was also explored using scanning electron microscopy. Moreover, the changes in the micropores of the MICP-treated sands were analyzed. From the findings of this paper, the following conclusions can be drawn.

- The creep deformation of the MICP-treated silica sands first enlarges and then declines as the number of grouting increases. The creep deformation of the MICP-treated silica sands grouted three and six times is more significant than that of the untreated silica sand. However, the creep deformation of the MICP-treated silica sand grouted nine times is 88.0% lower than that of the untreated silica sand, indicating that sufficiently treating the silica sand with the microbial-induced calcite precipitation declines its creep deformation.

- The creep characteristics of the MICP-treated calcareous sand are similar to those of the MICP-treated silica sand. The creep deformation of the MICP-treated calcareous sand first increases and then decreases as the number of grouting rises. However, the creep deformation of the MICP-treated calcareous sand is larger than that of the untreated calcareous sand except for the sand sample grouted three times, which has a creep deformation equivalent to that of the untreated calcareous sand. This result indicates that the treatment of the calcareous sand with the microbial-induced calcite precipitation positively affects its creep deformation.

- The SEM images demonstrate that the calcium carbonate formed by microorganisms in the voids creates a bonding between the sand particles, which enhances the integrity of the sand. This mechanism is identified as the key factor affecting the creep behavior of the MICP-treated silica sand. In contrast, in the case of the calcareous sand, the cavities on the surface of the calcareous sand particles are filled up with the formed calcium carbonate, which decreases the effect of the interlocking structure of the sand particles, thereby having a detrimental impact on maintaining a
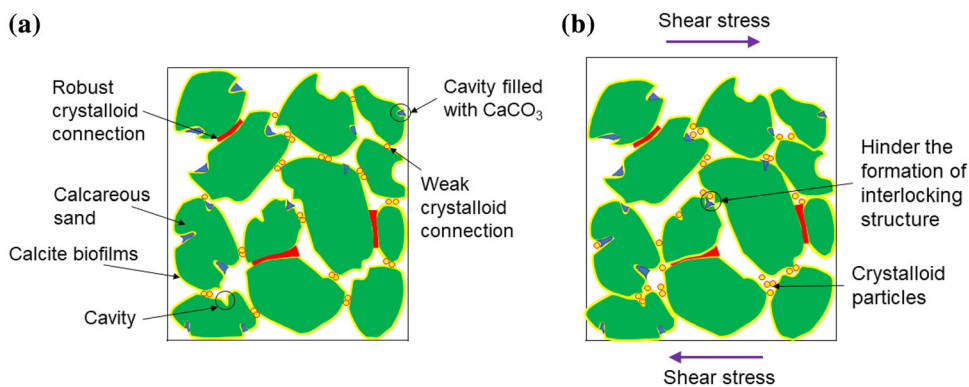

Fig. 18 Mechanisms of MICP-treated calcareous sand creep deformation **a** before loaded up to a given shear stress; **b** reach a new stable state

stable structure of the MICP-treated calcareous sand. Thus, the creep deformation of the calcareous sand treated with the microbial-induced calcite precipitation enlarges.

These findings provide a theoretical basis for reducing the long-term deformation of sand foundations by treating sand with microbial-induced calcite precipitation in practical engineering. The MICP treatment technology has good application prospects and is expected to replace traditional chemical reinforcement methods. At present, the research on the MICP treatment technology is primarily applied to sand, and the treatment of other types of soil, such as expansive soil and clay, with MICP should be investigated in the future.

Appendix

See Table 5.

Table 5 List of symbols

Symbol	Physical meaning	Unit
G_s	Specific gravity of soil particles	
d_{10}	Effective diameter	mm
d_{30}	Median diameter	mm
d_{60}	Constrained diameters	mm
C_u	Uniformity coefficient	
C_c	Coefficient of curvature	
e_{max}	Maximum void ratio	
e_{min}	Minimum void ratio	
OD_{600}	The optical density of the bacterial solution measured at a wavelength of 600 nm	
D_r	Relative compactness	
c	Cohesion	kPa
φ	Friction angle	°

Author Contributions Conceptualization, JY and XF; methodology, HT; software, DL and JZ; validation, JY and YS; formal analysis, DL and YS; investigation, DL and JZ; resources, JY and HT; data curation, DL and XF; writing—original draft preparation, JY and XF; writing—review and editing, JY; visualization, DL; supervision, HT and YS; project administration, YS and JY; funding acquisition, YS and JY. All authors have read and agreed to the published version of the manuscript.

Declarations

Conflict of Interest The authors declare no conflict of interest.

Data Availability The data presented in this study are available in J.Y., D.L., Y.S., H.T., X.F., J.Z. Direct Shear Creep Characteristics of Sand Treated with Microbial-Induced Calcite Precipitation.

References

1. Almajed A, Lateef MA, Moghal AAB, Lemboye K (2021) State-of-the-art review of the applicability and challenges of microbial-induced calcite precipitation (MICP) and enzyme-induced calcite precipitation (EICP) techniques for geotechnical and geoenvironmental applications. Curr Comput-Aided Drug Des 11:370. https://doi.org/10.3390/cryst11040370

2. Chu J, Ivanov V, He J, Naeimi M, Li B, Stabnikov V (2011) Development of microbial geotechnology in Singapore. Geo-Front 2011 Adv Geotech Eng. https://doi.org/10.1061/41165(397)416

3. Whiffin VS (2004) Microbial CaCO$_3$ precipitation for the production of biocement. PhD thesis, Murdoch University, Western Australia

4. Soltani-Jigheh H, Ghorbani M, Pazhouhandeh M, Emami Azadi M (2020) Bacterial treatment of remoulded fine-grained cohesive soils. Int J Civ Eng 18:463–473. https://doi.org/10.1007/s40999-019-00489-0

5. Montoya B, DeJong J (2015) Stress-strain behavior of sands cemented by microbially induced calcite precipitation. J Geotech Geoenviron Eng 141:04015019. https://doi.org/10.1061/(ASCE)GT.1943-5606.0001302

6. Mortensen B, DeJong J (2011) Strength and stiffness of MICP treated sand subjected to various stress paths. Geo-Front Adv Geotech Eng. https://doi.org/10.1061/41165(397)410

7. Zhao J, Tong H, Shan Y, Yuan J, Peng Q, Liang J (2021) Effects of different types of fibers on the physical and mechanical properties of MICP-treated calcareous sand. Materials 14:268. https://doi.org/10.3390/ma14020268

8. Zhao Q, Li L, Li C, Li M, Amini F, Zhang H (2014) Factors affecting improvement of engineering properties of MICP-treated soil catalyzed by bacteria and urease. J Mater Civ Eng 26:04014094. https://doi.org/10.1061/(ASCE)MT.1943-5533.0001013

9. Hataf N, Baharifard A (2020) Reducing soil permeability using microbial induced carbonate precipitation (MICP) method: A case study of shiraz landfill soil. Geomicrobiol J 37:147–158. https://doi.org/10.1080/01490451.2019.1678703

10. Kirkland CM, Thane A, Hiebert R, Hyatt R, Kirksey J, Cunningham AB, Gerlach R, Spangler L, Phillips AJ (2020) Addressing wellbore integrity and thief zone permeability using microbially-induced calcium carbonate precipitation (MICP): a field demonstration. J Petrol Sci Eng 190:107060. https://doi.org/10.1016/j.petrol.2020.107060

11. Zamani A, Montoya BM (2016) Permeability reduction due to microbial induced calcite precipitation in sand. Geo-Chicago 2016. https://doi.org/10.1061/9780784480120.011

12. Zamani A, Montoya BM (2017) Shearing and hydraulic behavior of MICP treated silty sand. Geotech Front 2017. https://doi.org/10.1061/9780784480489.029

13. Montoya B, DeJong J, Boulanger RW, Wilson DW, Gerhard R, Ganchenko A, Chou J-C (2012) Liquefaction mitigation using microbial induced calcite precipitation. GeoCongress 2012 State Art Practice Geotech Eng. https://doi.org/10.1061/9780784412121.197

14. Riveros GA, Sadrekarimi A (2020) Liquefaction resistance of Fraser River sand improved by a microbially-induced cementation. Soil Dyn Earthq Eng 131:106034. https://doi.org/10.1016/j.soildyn.2020.106034

15. Xiao P, Liu H, Xiao Y, Stuedlein AW, Evans TM (2018) Liquefaction resistance of bio-cemented calcareous sand. Soil Dyn Earthq Eng 107:9–19. https://doi.org/10.1016/j.soildyn.2018.01.008

16. Wang Z, Zhang N, Jin Y, Li Q, Xu J (2020) Application of microbially induced calcium carbonate precipitation (MICP) in sand embankments for scouring/erosion control. Mar Georesour Geotechnol. https://doi.org/10.1080/1064119X.2020.1850949

17. Chittoori BC, Rahman T, Burbank M, Moghal AAB (2019) Evaluating shallow mixing protocols as application methods for microbial induced calcite precipitation targeting expansive soil treatment. Proc Geo-Congress 2019 Soil Improv. 250:259. https://doi.org/10.1061/9780784482117.025

18. Baziar MH, Sanaie M, Amirabadi OE (2021) Mitigation of dust emissions of silty sand induced by wind erosion using natural soybean biomaterial. Int J Civ Eng 19:595–606. https://doi.org/10.1007/s40999-020-00587-4

19. Long Z, Cheng Y, Yang G, Yang D, Xu Y (2021) Study on triaxial creep test and constitutive model of compacted red clay. Int J Civ Eng 19:517–531. https://doi.org/10.1007/s40999-020-00572-x

20. Vallet A, Charlier J, Fabbri O, Bertrand C, Carry N, Mudry J (2016) Functioning and precipitation-displacement modelling of rainfall-induced deep-seated landslides subject to creep deformation. Landslides 13:653–670. https://doi.org/10.1007/s10346-015-0592-3

21. Sasaki Y, Fujii A, Asai K (2000) Soil creep process and its role in debris slide generation—field measurements on the north side of Tsukuba Mountain in Japan. Dev Geotech Eng Elsevier 84:199–219. https://doi.org/10.1016/S0165-1250(00)80017-6

22. Briaud J-L, Gibbens R (1999) Behavior of five large spread footings in sand. J Geotech Geoenviron Eng 125:787–796. https://doi.org/10.1061/(ASCE)1090-0241(1999)125:9(787)

23. Burland J, Burbidge M, Wilson E, TERZAGHI, (1985) Settlement of foundations on sand and gravel. Proc Inst Civ Eng 78:1325–1381. https://doi.org/10.1680/iicep.1985.1058

24. Du D-N, Wang L-G, Zhang X-D, Zhang S-K (2017) Study on sand particles creep model and open pit mine landslide mechanism caused by sand fatigue liquefaction. Proc IOP Conf Series Earth Environ Sci. https://doi.org/10.1088/1755-1315/69/1/012021

25. Arboleda-Monsalve LG, Zapata-Medina DG, Galeano-Parra DI (2019) Compressibility of biocemented loose sands under constant rate of strain, loading, and pseudo K0-triaxial conditions. Soils Found 59:1440–1455. https://doi.org/10.1016/j.sandf.2019.06.008

26. Xiao Y, Zhao C, Sun Y, Wang S, Wu H, Chen H, Liu H (2021) Compression behavior of MICP-treated sand with various gradations. Acta Geotech 16:1391–1400. https://doi.org/10.1007/s11440-020-01116-2

27. Feng K, Montoya B (2015) Drained shear strength of MICP sand at varying cementation levels. IFCEE 2015. https://doi.org/10.1061/9780784479087.208

28. Van Paassen LA (2009) Biogrout, ground improvement by microbial induced carbonate precipitation. PhD thesis, Delft University of Technology, Delft

29. Li M, Li L, Ogbonnaya U, Wen K, Tian A, Amini F (2016) Influence of fiber addition on mechanical properties of MICP-treated sand. J Mater Civ Eng 28:04015166. https://doi.org/10.1061/(ASCE)MT.1943-5533.0001442

30. DeJong J, Soga K, Kavazanjian E, Burns S, Van Paassen L, Al Qabany A, Aydilek A, Bang S, Burbank M, Caslake LF (2014) Biogeochemical processes and geotechnical applications: progress, opportunities and challenges. Pro Bio- Chemo-Mech Process Geotech Eng Géotech Symp Print 2013. https://doi.org/10.1680/bcmpge.60531.014

31. Yasuhara H, Neupane D, Hayashi K, Okamura M (2012) Experiments and predictions of physical properties of sand cemented by enzymatically-induced carbonate precipitation. Soils Found 52:539–549. https://doi.org/10.1016/j.sandf.2012.05.011

32. Harkes MP, van Paassen LA, Booster JL, Whiffin VS, van Loosdrecht MCM (2010) Fixation and distribution of bacterial activity in sand to induce carbonate precipitation for ground reinforcement. Ecol Eng 36:112–117. https://doi.org/10.1016/j.ecoleng.2009.01.004

33. Whiffin VS, Van Paassen LA, Harkes MP (2007) Microbial carbonate precipitation as a soil improvement technique. Geomicrobiol J 24:417–423. https://doi.org/10.1080/01490450701436505

34. Gu R, Fang Y (2006) An improved soil direct shear creep apparatus and its application. Chin J Rock Mech Eng 25:S2

35. Press, C.P. (2019) Standard for geotechnical test method (GBT 50123-2019).

36. Zhao M-H, Xiao Y, Chen C-F (2004) Laboratory experiment of the rheological property of soft clay and the improved xiyuan model. J Hunan Univ (Nat Sci) 1:48–51

37. Karimpour H, Lade PV (2010) Time effects relate to crushing in sand. J Geotech Geoenviron Eng 136:1209–1219. https://doi.org/10.1061/(ASCE)GT.1943-5606.0000335

38. Moghal AAB, Lateef MA, Abu Sayeed Mohammed S, Ahmad M, Usman AR, Almajed A (2020) Heavy metal immobilization studies and enhancement in geotechnical properties of cohesive soils by EICP technique. Appl Sci 10:7568. https://doi.org/10.3390/app10217568

39. Moghal AAB, Lateef MA, Mohammed SAS, Lemboye K, Chittoori B, Almajed A (2020) Efficacy of enzymatically induced calcium carbonate precipitation in the retention of heavy metal ions. Sustainability 12:7019. https://doi.org/10.3390/su12177019

40. Enomoto T, Koseki J, Tatsuoka F, Sato T (2015) Creep failure of sands exhibiting various viscosity types and its simulation. Soils Found 55:1346–1363. https://doi.org/10.1016/j.sandf.2015.10.002

41. Wang Y, Ma L, Wang M, Lv Y, Dong L, Fan P (2018) A creep constitutive model incorporating deformation mechanisms for crushable calcareous sand. Arab J Geosci 11:1–8. https://doi.org/10.1007/s12517-018-3982-8